Acta Oceanol. Sin., 2021, Vol. 40, No. 1, P. 13–21
https://doi.org/10.1007/s13131-020-1682-1
http://www.hyxb.org.cn
E-mail: hyxbe@263.net

Sea surface wind speed retrieval from Sentinel-1 HH polarization data using conventional and neural network methods

Tingting Qin[1, 2], Tong Jia[2, 3], Qian Feng[4], Xiaoming Li[2]*

[1] College of Surveying, Mapping and Geoinformation, Guilin University of Technology, Guilin 541006, China

[2] Key Laboratory of Digital Earth Science, Aerospace Information Research Institute, Chinese Academy of Sciences, Beijing 100094, China

[3] University of Chinese Academy of Sciences, Beijing 101408, China

[4] Key Laboratory of Space Ocean Remote Sensing and Applications, National Satellite Ocean Application Service, Beijing 100081, China

Received 5 January 2020; accepted 26 May 2020

Abstract

Conventional retrieval and neural network methods are used simultaneously to retrieve sea surface wind speed (SSWS) from HH-polarized Sentinel-1 (S1) SAR images. The Polarization Ratio (PR) models combined with the CMOD5.N Geophysical Model Function (GMF) is used for SSWS retrieval from the HH-polarized SAR data. We compared different PR models developed based on previous C-band SAR data in HH-polarization for their applications to the S1 SAR data. The recently proposed CMODH, i.e., retrieving SSWS directly from the HH-polarized S1 data is also validated. The results indicate that the CMODH model performs better than results achieved using the PR models. We proposed a neural network method based on the backward propagation (BP) neural network to retrieve SSWS from the S1 HH-polarized data. The SSWS retrieved using the BP neural network model agrees better with the buoy measurements and ASCAT dataset than the results achieved using the conventional methods. Compared to the buoy measurements, the bias, root mean square error (RMSE) and scatter index (SI) of wind speed retrieved by the BP neural network model are 0.10 m/s, 1.38 m/s and 19.85%, respectively, while compared to the ASCAT dataset the three parameters of training set are –0.01 m/s, 1.33 m/s and 15.10%, respectively. It is suggested that the BP neural network model has a potential application in retrieving SSWS from Sentinel-1 images acquired at HH-polarization.

Key words: Sentinel-1, HH-polarization, sea surface wind speed, retrieval methods

Citation: Qin Tingting, Jia Tong, Feng Qian, Li Xiaoming. 2021. Sea surface wind speed retrieval from Sentinel-1 HH polarization data using conventional and neural network methods. Acta Oceanologica Sinica, 40(1): 13–21, doi: 10.1007/s13131-020-1682-1

1 Introduction

Sea surface wind (SSW) is the major force of global ocean circulation (Pond and Pickard, 1983). SSW field data with high spatial resolution play an important role in meteorological prediction, ship detection, maritime transportation and accidents rescue. Traditional methods of measuring sea surface wind speed (SSWS), such as buoys, wind towers, meteorological stations and ships, cannot meet the needs of real-time and fast acquisition of regional or global scale SSW field (Pierson, 1990). With the rapid development of satellite remote sensing technology, microwave scatterometer, microwave radiometer and synthetic aperture radar (SAR) become effective approaches to obtain regional-scale high spatial resolution SSWS.

SAR has distinctive advantages in SSWS retrieval due to its all-day, all-weather and high-resolution characteristics. In general, SAR data in VV polarization are more widely applied in oceanography research than the data in HH polarization, because the sea surface backscatter in VV polarization is stronger than that in HH polarization. However, in maritime surveillance (e.g., in sea-ice monitoring and oil-spill detection), SAR data in HH polarization are demanded (Komarov and Buehner, 2017). Under such circumstance, it is required to use the HH-polarization SAR to derive SSWS, which can be integrated with the detected targets to be provided to end users.

There are generally two ways to retrieve SSWS by the HH-polarization SAR data. The routinely used way is to transform the normalized radar cross section (NRCS) of HH-polarization to that of VV-polarization by using polarization ratio (PR) model, and then use CMOD Geophysical Model Functions (GMF) to retrieve the SSWS. Often used C-band GMF for VV polarization data of Scatterometers and SARs includes CMOD4 (Stoffelen and Anderson, 1997), CMOD_IFR2 (Quilfen et al., 1998), CMOD5 (Hersbach et al., 2007) and CMOD5.N (Hersbach, 2010), etc. Elfouhaily (1996) proposed the first PR model. Since then, based on different SAR data, several PR models which hold that PR is dependent on the incidence angle have been proposed, e.g., the Zhang-PR model (Zhang et al., 2011), Mouche-PR2 (Mouche et al., 2005) model and Liu-PR model (Liu et al., 2013). In addition to the in-

Foundation item: The National Key Research and Development Program under contract Nos 2016YFC1402703 and 2018YFC1407100.
*Corresponding author, E-mail: lixm@radi.ac.cn

cidence angle dependence, Mouche et al. (2005) found that the PR is also dependent on the wind direction. Therefore, a new PR model containing both the incidence angle and the wind direction is developed, hereinafter referred to as Mouche-PR1 model. Based on more SAR data and other collocated measurements available, it is found that wind speeds should also be taken into account in the PR models (Zhang et al., 2010). The other way to retrieve SSWS by the HH-polarization SAR data is to establish GMF suitable for HH polarization of SAR data to directly retrieve SSWS. Monaldo et al. (2004) attempted to generate a new C-band HH polarization model function by using the CMOD4 GMF and grafting on a PR function based on the RADARSAT-1 SAR wind and QuikSCAT scatterometer wind. Later, Zhang et al. (2019) used ENVISAT ASAR collocated with ASCAT winds to derive a GMF for HH polarization of SAR data based on CMOD5, hereinafter referred to as CMODH model.

Neural network is a method of data analysis that automates analytical model building. For neural network method applied in SSWS retrieval, the most recent research, devoted to retrieving SSW field of scatterometer using neural network, can date back to Thiria et al. (1993). Afterwards, Richaume et al. (2000) applied the similar architectures to retrieve SSW from spaceborne ERS-1 SCAT data. The neural network method has also been applied to spaceborne SAR data to retrieve SSW, e.g., presented by Horstmann et al. (2003) and Wang et al. (2017).

Sentinel-1 C-band SAR is the radar satellite of the Europe Space Agency (ESA) Copernicus Program, which consists of Sentinel-1A (launched in April 2014) and Sentinel-1B (launched in April 2016). The Sentinel-1 SAR instruments support operation in single polarisation (HH or VV) and dual polarisation (HH+HV or VV+VH). It can acquire data in four imaging modes of stripmap (SM), interferometric wide swath (IW), extra wide swath (EW) and wave mode (WV). The revisit period of its single satellite (Sentinel-1A or Sentinel-1B) is 12 d. After the two satellites are in orbit at the same time, the revisit period is shortened to 6 d. Therefore, Sentinel-1 plays an important role in the dynamical monitoring of marine environment. In the Arctic region, Sentinel-1 acquires a large amount of HH-polarization data for sea ice monitoring. In order to better serve the monitoring of the Arctic marine environment, systematic research and comparative analysis are needed to obtain the most suitable method for Sentinel-1 HH polarization SAR SSW. In this study, we firstly compared the four PR models (Mouche-PR1 models, Mouche-PR2 model, Zhang-PR model and Liu-PR model) mentioned above and their combination with CMOD5.N GMF to retrieve SSWS. Further, the recently proposed CMODH GMF was investigated. Finally, we proposed a new method of retrieving SSWS by Sentinel-1 HH polarized data based on the back propagation neural network (BPNN).

In Section 2, we briefly introduce the dataset and the retrieval SSWS methods used in this study. In Section 3, comparisons of the SSWS retrieval from Sentinel-1 HH polarized data using different PR models, CMODH and the proposed BP neural network algorithm are conducted. A preliminary conclusion is given in Section 4.

2 Datasets and methodology

2.1 *Data and processing*

2.1.1 *Sentinel-1 SAR data*

Table 1 lists the main technical parameters of the Sentinel-1 data used in this study.

The processes applied to the Sentinel-1 data prior to retrieving SSWS include radiometric calibration, thermal noise elimination and data resampling. The radiometric calibration and thermal noise elimination process of Sentinel-1 data are shown below (ESA, 2016).

$$\sigma^0_{\mathrm{HH}}(i) = \frac{\mathrm{DN}_i^2 - \eta_i}{A_i^2}, \tag{1}$$

where DN_i is the digital number of i-th pixel in the image, A_i is the sigma nought (i) and η_i is the noiseLut (i).

The unavoidable existence of speckles in the SAR image makes it impossible to retrieve wind speed at the primary pixel resolution. Therefore, prior to the SSWS retrieval from Sentinel-1 data using the small cell size, we assess the speckle "noise" in the cells as the result of averaging multiple pixels. In this study, the radiometric resolution (γ) defined in Eq. (2) is used to describe the speckle "noise" (Olivier and Vidal-Madjar, 1994).

$$\gamma = 10\log_{10}\left(1 + \frac{1}{\sqrt{\mathrm{ENL}}}\right), \tag{2}$$

where ENL means the equivalent number of looks, given as Eq. (3):

$$\mathrm{ENL} = \frac{(E[P])^2}{\mathrm{VAR}[P]}, \tag{3}$$

where P is the intensity of pixel from the image, and VAR and E are the mean and variance of P, respectively (Moreira, 1991).

In this study, 2 277 scenes of Sentinel-1 HH polarization data were collocated with the ASCAT data, which is described in detail in Section 2.1.3. Based on the 2 277 scenes, we evaluated the radiometric resolution along with sub-scene size (i.e., cell size) used for SSWS retrieval. Each sub-scene is sampled from 200 m× 200 m to 6 km×6 km and the corresponding statistical result is shown in Fig. 1. As seen from the Fig. 1, the radiometric resolution decreases with the increase of cell size. When the cell size decreases from 200 m×200 m to 2 km×2 km, the radiometric resolution decreases rapidly, and tends to decrease gently between 2 km×2 km and 6 km×6 km. The average of radiometric resolution ranges from 0.31 dB to 0.58 dB, and the standard deviation fluctuates from 0.08 dB to 0.12 dB. Furthermore, the radiometric resolution in the grid size of 1 km×1 km to 6 km×6 km is below the absolute calibration accuracy (0.43 dB) of the Sentinel-1 data (Schwerdt et al., 2014). Therefore, the size of 2 km by 2 km with small error of radiometric resolution and high spatial resolution

Table 1. Technical specifications of Sentinel-1 IW and EW modes

Mode	Incidence angle/(°)	Nominal resolution	Swath width/km	Polarization
IW	29–46	5 m×20 m	250	HH+HV, HH, VH+VV, VV
EW	19–47	25 m×40 m	400	HH+HV, HH, VH+VV, VV

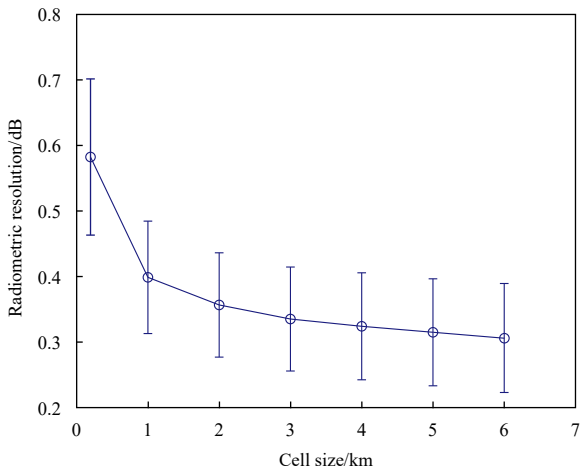

Fig. 1. Geographical locations of the Sentinel-1 and buoy data in this study.

is used for the following analysis of sea surface wind retrieval.

2.1.2 *In situ buoy data*

In the presented study, 130 Sentinel-1 data acquired in HH polarization in EW and IW mode from October 2014 to December 2018 were collected, which are matched-up with the buoys, as presented in Fig. 2a. The buoy measurements are used to validate the Sentinel-1 retrieved SSWS.

The buoy dataset was released by the National Data Buoy Center (NDBC), which are collocated with the Sentinel-1 images within a temporal window of less than 10 min for the validation of HH-polarization retrieved wind speeds. The black solid points in Fig. 2a indicate the positions of NDBC buoys and the related information such as buoy ID, longitude and latitude, and anemometer altitude is given in Table 2. Note that the buoy measurements of wind speed referenced at anemometer heights, need to be converted to those at 10 m height above the sea surface, in order to be consistent with the SAR retrievals. In this study, the Peixoto and Oort (1992) method is used to convert the wind

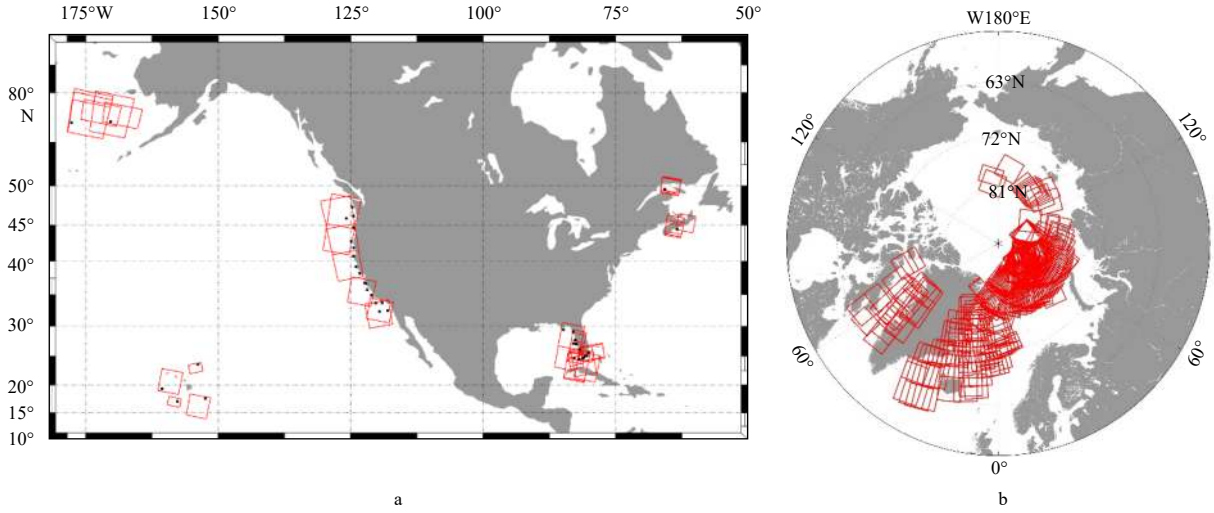

Fig. 2. The calculated radiometric resolution as a function of cell sizes based on a dataset of 2 277 scenes of Sentinel-1 HH polarization data.

Table 2. Information table of buoy data used in this study

Station	Latitude	Longitude	Height/m	Station	Latitude	Longitude	Height/m
46022	40.720°N	124.531°W	4	46047	32.398°N	119.498°W	5
46014	39.233°N	123.967°W	4	46029	46.143°N	124.485°W	5
46013	38.238°N	123.307°W	4	46041	47.353°N	124.742°W	5
46015	42.779°N	124.874°W	4	51003	19.289°N	160.569°W	5
46050	44.677°N	124.515°W	4	51000	23.535°N	153.781°W	5
46092	36.751°N	122.029°W	4	44258	44.500°N	63.400°W	5
46025	33.749°N	119.053°W	4	45138	49.540°N	65.710°W	5
51004	17.602°N	152.395°W	4	SMKF1	24.628°N	81.109°W	6.1
32303	5.000°N	95.000°W	4	VCAF1	24.711°N	81.107°W	6.5
43301	8.000°N	95.000°W	4	NPSF1	26.132°N	81.807°W	6.5
51002	17.037°N	157.696°W	4	MTBF1	27.661°N	82.594°W	6.7
46035	57.026°N	177.738°W	5	LONF1	24.844°N	80.864°W	7
46027	41.852°N	124.382°W	5	VCVA2	57.125°N	170.285°W	8.5
46089	45.925°N	125.771°W	5	CDRF1	29.136°N	83.029°W	10
46011	34.956°N	121.019°W	5	VENF1	27.072°N	82.453°W	11.6
46028	35.712°N	121.858°W	5	SANF1	24.456°N	81.877°W	14.6
46042	36.785°N	122.398°W	5	MLRF1	25.012°N	80.376°W	15.8
46069	33.674°N	120.212°W	5	PLSF1	24.693°N	82.773°W	17.7
46086	32.491°N	118.035°W	5				

speed measured at 10 m height which is given as:

$$\frac{U}{U_{\mathrm{m}}}=\frac{\mathrm{in}\left(Z/Z_0\right)}{\mathrm{in}\left(Z_{\mathrm{m}}/Z_0\right)}, \tag{4}$$

where U is the wind speed at height Z, U_{m} is the wind speed at height Z_{m} (i.e., the wind speed measured by buoys), Z_0 is the roughness length with the value of 1.52×10^{-4} m.

2.1.3 *Scatterometer ASCAT data*

ASCAT is a spaceborne C-band scatterometer which was launched on the European Organization for the Exploitation of Meteorological Satellites (EUMETSAT) MetOp-A satellite in October 2006. Another ASCAT instrument became operational on MetOp-B when launched in September 2012. ASCAT operates at a frequency of 5.255 GHz (C-band) and uses a vertically polarized antenna, whose primary objective is to measure wind speed and direction over the oceans. In this study, the daily EUMETSAT ASCAT-A/B wind data at 10 m under all-weather conditions with a spatial resolution of 0.25° by 0.25° were used for comparison with the Sentinel-1 wind retrievals. The ASCAT wind products were collocated with the Sentinel-1 SAR sub-scenes within a spatial window of 25 km and a temporal window of less of 1.5 h for the validation of HH polarization retrieved SSWS.

A total of 2 277 Sentinel-1 data acquired in EW mode in the Arctic Ocean from June to December 2018 were matched-up with the ASCAT (A and B) data. Spatial distribution of the Sentinel-1 data is shown in Fig. 2b.

2.1.4 *ERA5 reanalysis data*

The ERA5 dataset is a global climate reanalysis model dataset, which was released by the European Center for Medium-Range Weather Forecasts (ECMWF). The ERA5 reanalysis data have a grid size of 0.25° and are available every one hour.

2.2 *Method of the SSWS retrieval from Sentinel-1 HH-polarized data*

2.2.1 *Using the PR models*

GMF describes the relationship between radar backscattering coefficient and radar incidence angle, the 10-m height surface wind, which is widely used to retrieve SSW from microwave scatterometer and SAR data. At present, CMOD5 and CMOD5.N are widely used in GMF. Since CMOD5.N corrects the 0.5 m/s deviation caused by the neutral wind, which better describes the sea surface condition compared with CMOD5. Therefore, the CMOD5.N function is used in this study to retrieve SSWS which is given as (Hersbach, 2010):

$$\begin{aligned}\sigma_0^{\mathrm{VV}}\left(\theta,\phi,u_{10}\right)=&a_0\left(\theta,u_{10}\right)\left[1+a_1\left(\theta,u_{10}\right)\cos\phi+\right.\\&\left.a_2\left(\theta,u_{10}\right)\cos2\phi\right]^p,\end{aligned} \tag{5}$$

where σ_0 is the normalized backscatter in linear unit. The terms a_0, a_1 and a_2 are functions of SSWS (u_{10}) and the incidence angle (θ). ϕ is the azimuth angle between the radar look direction (α) and the wind direction (χ), i.e., $\phi=\chi-\alpha$. p is a parameter with a value of 1.6.

The abovementioned CMOD5.N function is applicable to SAR data in VV-polarization. Therefore, when the SAR data in HH-polarization are used for SSW retrieval, we need to transform the NRCS of the HH-polarization to that of the VV-polarization by using a PR model. The PR is described as the ratio of VV NRCS to HH NRCS in a linear unit, given as:

$$\mathrm{PR}=\frac{\sigma_{\mathrm{VV}}^0}{\sigma_{\mathrm{HH}}^0}. \tag{6}$$

In this study, four PR models, including Mouche-PR1 model (Mouche et al., 2005), Mouche-PR2 model (Mouche et al., 2005), Zhang-PR model (Zhang et al., 2011) and Liu-PR model (Liu et al., 2013), are considered to retrieve SSWS for the Sentinel-1 data.

Mouche-PR1 model is a PR model depending on incident angle and azimuth angle and determined based on ENVISAT ASAR data, as given in Eq. (7):

$$\mathrm{PR}\left(\theta,\phi\right)=C_0\left(\theta\right)+C_1\left(\theta\right)\cos\left(\phi\right)+C_2\left(\theta\right)\cos\left(2\phi\right), \tag{7}$$

where the coefficients C_0, C_1, and C_2 correspond to the upwind ($\phi=0$), crosswind ($\phi=\pi/2$), and downwind ($\phi=\pi$) directions (Eqs (8) – (10)), respectively.

$$C_0\left(\theta\right)=\left(\mathrm{PR}\left(\theta,0\right)+\mathrm{PR}\left(\theta,\pi\right)+2\mathrm{PR}(\theta,\pi/2\,)\right)/4, \tag{8}$$

$$C_1\left(\theta\right)=\left(\mathrm{PR}\left(\theta,0\right)-\mathrm{PR}(\theta,\pi)\right)/2, \tag{9}$$

$$C_2\left(\theta\right)=\left(\mathrm{PR}(\theta,0)+\mathrm{PR}(\theta,\pi)-2\mathrm{PR}(\theta,\pi/2)\right)/4, \tag{10}$$

In Eqs (8)–(10), the $\mathrm{PR}(\theta,0)$, $\mathrm{PR}(\theta,\pi/2)$ and $\mathrm{PR}(\theta,\pi)$ can be derived by Eq. (11). The model coefficients are shown in Table 3.

$$\mathrm{PR}_\phi\left(\theta\right)=A_\phi\exp\left(B_\phi\theta\right)+C_\phi. \tag{11}$$

Zhang-PR model, Mouche-PR2 model and Liu-PR model are those depending on incident angle, as shown in Eq. (12):

$$\mathrm{PR}\left(\theta\right)=A\exp\left(B\theta\right)+C, \tag{12}$$

where θ is incident angle, A, B and C are constant coefficients. The coefficients of the three models are shown in Table 3. As Sentinel-1 SAR have not acquired data in VV and HH polarization, it is impossible to fit out an optimum PR model to retrieve SSWS from the Sentinel-1 HH-polarized data. Therefore, the coefficients listed in Table 4 are determined based on ENVISAT ASAR, RADARSAT-2 and ENVISAT ASAR data, respectively.

2.2.2 *Using the CMODH model*

The CMODH model (Zhang et al., 2019) is determined based on more than 2 700 ENVISAT/ASAR images acquired in wide

Table 3. Coefficients of Mouche-PR1 model

Coefficient	Value
A_0	0.006 507 04
B_0	0.128 983 00
C_0	0.992 839 00
$A_{\pi/2}$	0.007 821 94
$B_{\pi/2}$	0.121 405 00
$C_{\pi/2}$	0.992 839 00
A_π	0.005 984 16
B_π	0.140 952 00
C_π	0.992 885 00

Table 4. Coefficients of PR model with incidence angle dependence

PR model	*A*	*B*	*C*
Mouche-PR2	0.007 997 93	0.125 465	0.997 379
Zhang-PR	0.282 8	0.045 1	0.289 1
Liu-PR	0.453 041 0	0.032 457 3	0.524 303 0

swath mode (WSM) in 2009 collocated with ASCAT winds, which were used to directly retrieve SSWS, without considering NRCS transformation by using PR models. The form of the CMODH model is the same as that of CMOD5.N.

2.2.3 *Using the BPNN method*

Due to the complexity of ocean motion and the limitation of the theoretical model of electromagnetic scattering from sea surface, the imaging mechanism of SAR on the sea surface wind field is rather complicated. In fact, the SAR image obtained from the sea surface is a complex non-linear process (Yang, 2009). BP neural network method is a good tool for dealing with non-linear problems, therefore we consider the possibility of using BP neural network to retrieve SSWS from spaceborne SAR data.

BP neural network is a multi-layer feedforward neural network. The topological structure of the three-layer BP network is shown in Fig. 3. It consists of input layer, output layer and a hidden layer. Each neuron connects with all the neurons in the next layer, but there is no connection between the neurons in the same layer. The basic principle of BP neural network is to use gradient descent method to adjust weights and thresholds so as to minimize the mean square error of the actual output value and the expected output value of the network.

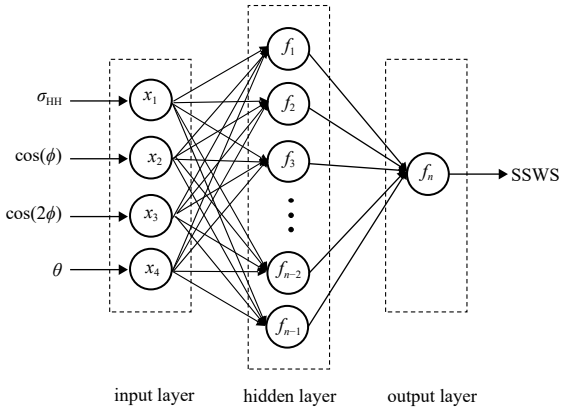

Fig. 3. The structure of three-layer BP neural network.

From expression of CMOD function (e.g., Eq. (5)), it can be seen that the SSWS retrieved by SAR is not only related to the backscattering coefficient, but also to the incident angle and azimuth angle of radar antenna. Therefore, there are four nodes in the input layer of BP neural network in this paper, including σ_{HH}, cos(ϕ), cos(2ϕ), θ. The output layer node of the network has only one value of wind speed. The hidden layer is set to three layers, and the number of hidden nodes is 6, 10 and 8, respectively. The transfer function of the hidden layer is "*tansig*" (tangent S-type transfer function), which can converge quickly. The output layer transfer function is "*purelin*" (linear transfer function), which can make the whole network output arbitrary values. The training function is "*traindx*" (momentum BP algorithm with variable learning rate), which has the fastest convergence speed for medium-scale BP network. The learning function of the network is "*learngdm*" (gradient descent momentum learning function), which is used to calculate the change rate of weights or thresholds. The performance function of the network is MSE (mean square error performance function), which is a fast way to measure the "average error".

Because of the difference in the magnitude range of the obtained σ_{HH}, cos(ϕ), cos(2ϕ), θ data, the network will not converge or the convergence speed will be slow, so before training the network, the input value (σ_{HH}, cos(ϕ), cos(2ϕ), θ) and output value (wind speed) of the model need to be normalized, as given in

$$X_i = \frac{x_i - x_{\min}}{x_{\max} - x_{\min}}, \tag{13}$$

where x_i is the input and output data, $x_{\max}$ and $x_{\min}$ are the maximum and minimum values of the input and output data, respectively, and X_i is the normalized input and output. After normalizing the data, we can begin to train the network using the designed network model. It is noted that the retrieved SSWS needs to be anti-normalized after training.

3 Results and analysis

3.1 *SSWS retrieval using conventional methods*

Taking the wind direction of buoy measurement as the actual value, the four PR models combined with CMOD5.N and CMODH model are used to retrieve SSWS from the HH-polarization Sentinel-1 data (their spatial coverages are shown in Fig. 2b). The retrieved SSWS then is compared with the matched buoy measurements of wind speed, which are shown in Fig. 4, respectively. The results show that, compared with the buoy measurements, the bias of SSWS retrieved from each PR model and CMODH model are less than 0.35 m/s. The bias of the Mouche-PR1 model, Mouch-PR2 model and Liu-PR model are positive, among which the Mouche-PR1 model is the smallest with value of 0.11 m/s. By contrast, the bias of Zhang-PR model and CMODH model are of –0.33 m/s and –0.31 m/s, respectively, which slightly underestimates the SSWS.

In order to further analyze and evaluate discrepancies of wind speed retrieval by different methods, the statistical parameters of the root mean square error (RMSE) and scatter index (SI) are calculated. We found that the results of CMODH model are slightly better than the corresponding results of the four PR models, which yields an RMSE and a SI of 1.48 m/s and 20.89%, respectively. In contrast, the Liu-PR model yields the largest RMSE and SI. The two parameters of the Liu-PR model are 1.78 m/s and 25.36%, respectively. The results of Mouche-PR1 model and Mouche-PR2 model are similar to each other, while the statistical parameters of Mouche-PR1 model considering wind direction and incident angle is slightly better than that of Mouche-PR2 model only considering incident angle.

Because only limited Sentinel-1 SAR data are matched with buoys, in order to further investigate the performance of the four PR models and CMODH model, the comparisons of the ASCAT measurements and Sentinel-1 SAR–derived SSWS are conducted based on the 2 277 scene Sentinel-1 data matching with ASCAT acquired in Arctic ocean. The comparison results are presented in Fig. 5. In these comparisons, we assume the wind direction of ASCAT as the real value and only the ASCAT wind vectors within coverage of the Sentinel-1 scenes were selected for analysis. All the retrieved SSWS of SAR sub-scenes (2 km by 2 km) within an ASCAT data grid (0.25° by 0.25°) are averaged to reduce variability for comparison with the numerical model results in coarse

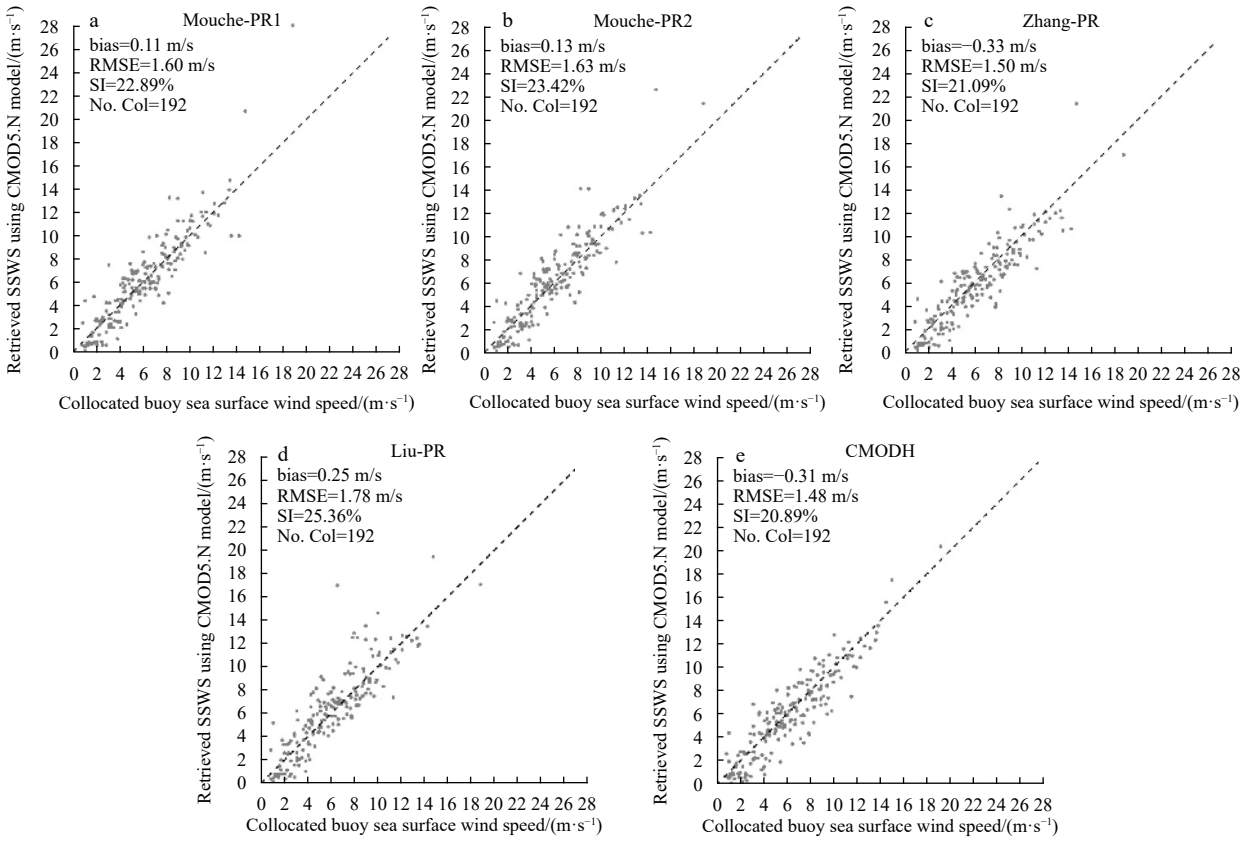

Fig. 4. Comparisons of the retrieved SSWS using the PR models of Mouche-PR1 (a), Mouche-PR2 (b), Zhang-PR (c) and Liu-PR (d) and CMODH (e) model with the collocated buoy wind speeds.

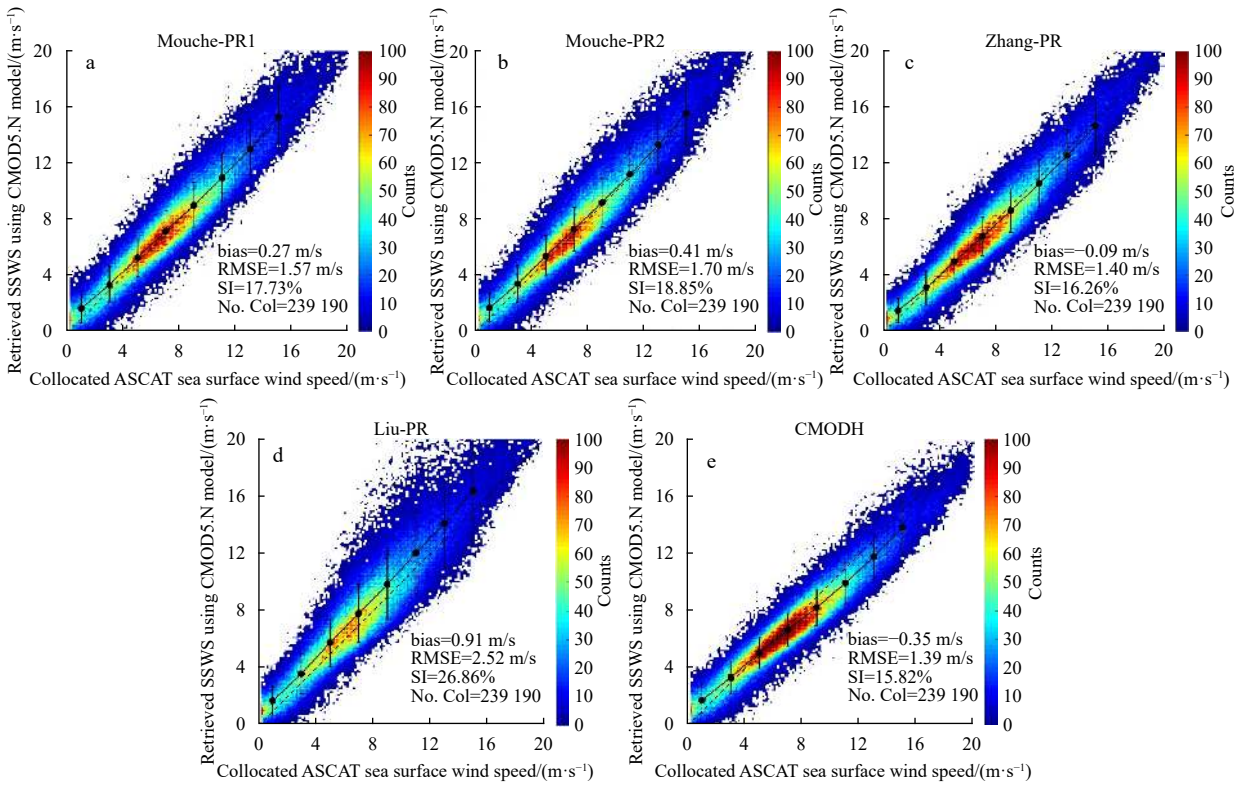

Fig. 5. Comparisons of the retrieved SSWS using the PR models of Mouche-PR1 (a), Mouche-PR2 (b), Zhang-PR (c) and Liu-PR (d) and CMODH model (e) with the collocated ASCAT wind speeds.

resolutions. The following comparative analyses with ASCAT are also conducted in this way. In Fig. 5, the color represents the amount of data in grids with a regular interval of 0.2 m/s. The results show that, compared with the ASCAT measurements, the RMSE and SI of CMODH model are the smallest with the value of 1.39 m/s and 15.82% respectively, which should attribute to coefficients of the CMODH model (Zhang et al., 2019) are determined based on ENVISAT/ASAR data and ASCAT data.

Considering the statistical parameters in terms of bias, RMSE and SI obtained by comparison with buoy measurements and ASCAT wind speed, as shown in Table 5, it is found that the SSWS retrieved by the four PR models combined with CMOD5.N and CMODH model are in good agreement with buoy measurements and ASCAT wind speed. Compared to buoy, the absolute bias of the five models is less than 0.5 m/s, and the RMSE fluctuates between 1.3 m/s and 1.8 m/s. While, compared to ASCAT, the absolute bias of the five models is less than 1m/s, and the RMSE fluctuates between 1.3 m/s and 2.6 m/s. Specially, CMODH model is better than the other PR models while retrieving the SSWS from Sentinel-1 HH-polarization data. This indicates that an independent GMF dedicated for the HH-polarized SAR data should perform better than the combination of PR model and GMF developed for VV-polarized data.

3.2 *SSWS retrieval using BPNN method*

In this method, 239 190 samples of σ_{HH}, $\cos(\phi)$, $\cos(2\phi)$, θ acquired in the Arctic ocean are input into the neural network. The number of iterations of the network is set to 50 000 times and the learning rate is 0.01. 80% of the data pairs matching with ASCAT data are randomly selected as training set and 20% are as test set. The weights of the network nodes are adjusted according to the experimental results, and the minimum RMSE is used as the standard to establish the optimal BP neural network for SSWS retrieval. The results of retrieving SSWS using the optimal BP neural network are shown in Figs 6a and b. Error bars are overlaid on the scatter plots and the majority of the data points lies between 3 m/s and 9 m/s. The statistical parameters of bias, RMSE and SI are shown in Table 5. The results show that the BP neural network can effectively retrieve SSWS from Sentinel-1 HH data. Its Bias, RMSE and SI of training set are 0.03 m/s, 1.33 m/s and 15.39%, respectively, and the test set are –0.01 m/s,1.33 m/s and 15.10%, respectively. Overall, the retrieval result of the BP neural network performs well although relative high bias appears in low wind speed, especially for SSWS less than 3 m/s. However, it needs to be pointed out that all these training and testing samples lack high wind speed samples (above 25 m/s). Therefore, we would like to collect more high wind speed data to improve our BP neural network retrieval accuracy in the future study.

Table 5. Statistical parameters of SSWS retrieval using different methods

	Models	Bias/(m·s^{-1})	RMSE/(m·s^{-1})	SI/%
Compared with buoy	Mouche-PR1	0.11	1.60	22.89
	Mouche-PR2	0.13	1.63	23.42
	Zhang-PR	–0.33	1.50	21.09
	Liu-PR	0.25	1.78	25.36
	CMODH	–0.31	1.48	20.89
	BPNN	0.10	1.38	19.85
Compared with ASCAT	Mouche-PR1	0.27	1.57	17.73
	Mouche-PR2	0.41	1.70	18.85
	Zhang-PR	–0.09	1.40	16.26
	Liu-PR	0.91	2.52	26.86
	CMODH	–0.35	1.39	15.82
	BPNN (training set)	0.03	1.33	15.39
	BPNN (test set)	–0.01	1.33	15.10

In order to further verify the feasibility of retrieving the SSWS of SAR using BP neural network, we choose the 130 Sentinel-1 SAR data matching with buoys to retrieve the SSWS by using the trained optimal BP neural network model, and compare the retrieved results with the buoys. The results are shown in Fig. 6c, and the statistical parameters of the bias, the RMSE and the SI are 0.10 m/s, 1.38 m/s, and 19.85%, respectively. The BP neural network SSWS retrieval accuracy is improved compared to the above-mentioned conventional methods. The interaction between backscattering coefficient, incident angle, azimuth angle of radar antenna and SSWS is a very complex non-linear relationship, which is suitably simulated with black box model such as neural network. Thus it is feasible to use the BP neural network method to retrieve the SSWS.

3.3 *An example of SSWS retrieval for Sentinel-1 HH polarization data using different methods*

In this paper, an example of SSWS retrieval using the conventional and neural network methods from Sentinel-1 HH polarization data are shown in Figs 7a–f. The SAR data were acquired at 06:41 UTC on 22 August 2017. The overlaid arrows indicate the ERA5 SSW on the same day. The external reference of wind directions used for SSWS retrieval are the collocated ERA5 reanalysis model wind directions. The average wind speed of ERA5 is 7.46 m/s,

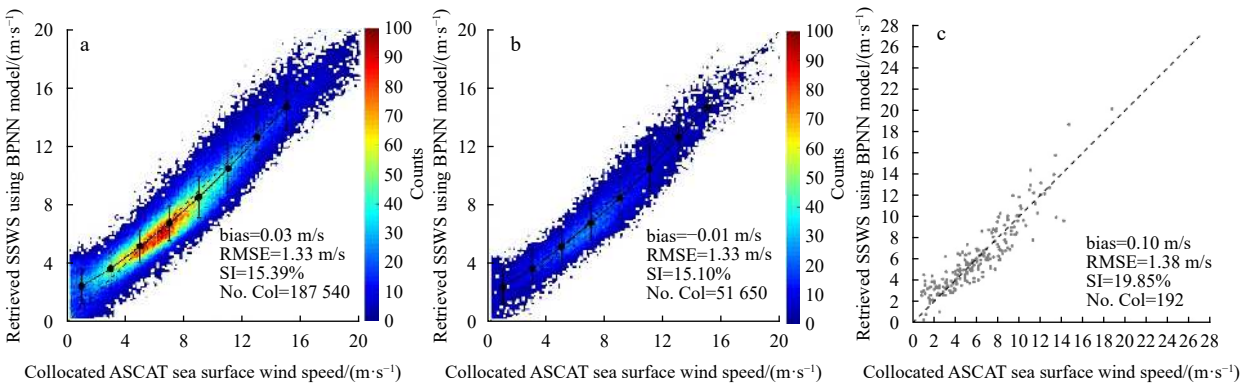

Fig. 6. Comparisons of the retrieved SSWS using the training set of BP neural network (a), the test set of BP neural network (b) and the trained optimal BP neural network (c) models with the collocated ASCAT and buoy wind speeds.

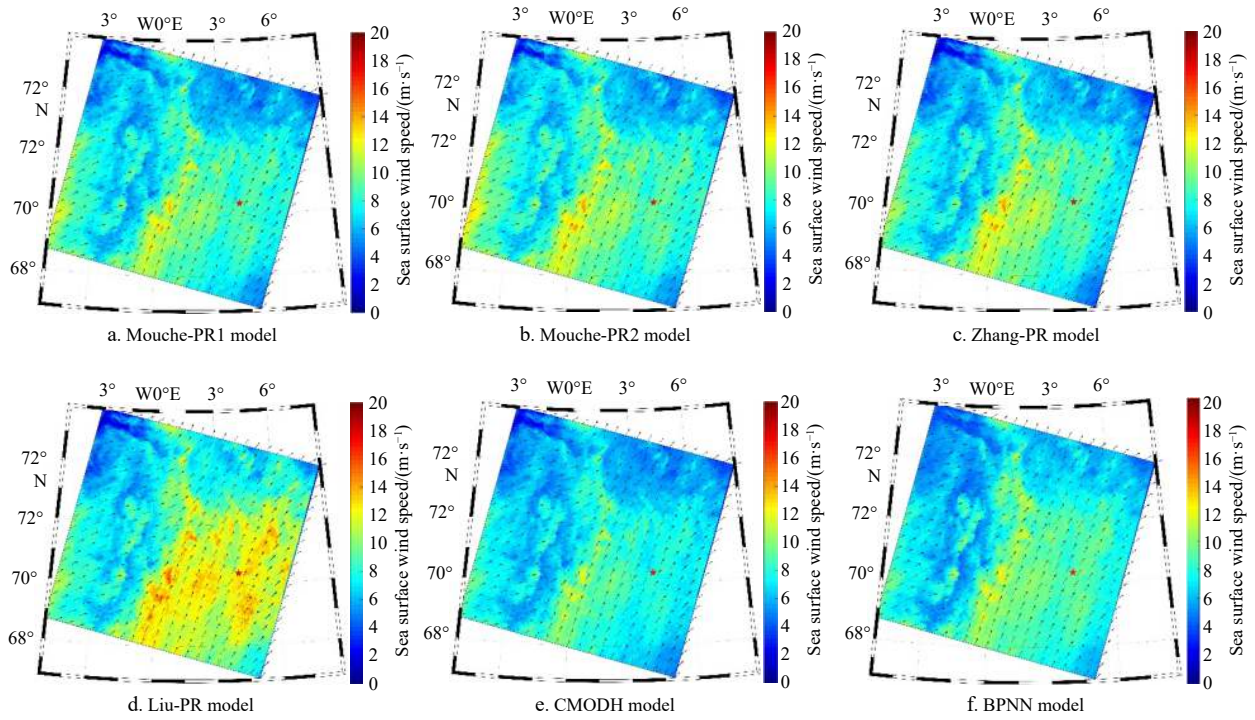

Fig. 7. An example of SSWS retrieval for Sentinel-1 HH polarization data using Mouche-PR1 model (a), Mouche-PR2 model (b), Zhang-PR model (c), Liu-PR model (d), CMODH model (e), and BP neural network model (f). The collocated ERA5 wind vectors within the coverage of the Sentinel-1 image are overlaid. The red pentagram marks the location of the R/V *Xuelong*.

and the average wind speed obtained by the 6 models (Mouche-PR1 model, Mouche-PR2 model, Zhang-PR model, Liu-PR model, CMODH model and BP neural network model) are 7.58 m/s, 7.99 m/s, 7.64 m/s, 9.11 m/s, 6.98 m/s and 7.53 m/s, respectively. This suggests that the overall value of the SAR-derived SSWS with the 6 models are close to each other. However, they do show some discrepancies of spatial variations, which is particularly evident in the retrieval by the Liu-PR model.

The red pentagram in the Figs 7a–f indicates the location of the R/V *Xuelong* at 06:41 UTC on 22 August 2017. The wind speed from the R/V *Xuelong* measurement at 20 m height is converted to the wind speed at 10 m height assuming neutral wind, which results in a value of 9.42 m/s. The wind direction acquired on *Xuelong* is about 222.8° (clockwise relative to North). The SAR-derived SSWS closest to the *Xuelong* location are 9.17 m/s for the Mouche-PR1 model, 9.46 m/s for the Mouche-PR2 model, 9.24 m/s for the Zhang-PR model, 13.29 m/s for the Liu-PR model, 8.21 m/s for the CMODH model and 9.50 m/s for the BP neural network model (based on a 2 km by 2 km subscene). Although the *in situ* measurement by *Xuelong* is only limited to a single location, the retrievals nevertheless with the Mouche-PR2 and the BP neural network methods have the best agreements with the *in situ* measurement. We are collecting more *in situ* data acquired in Arctic MIZ to validate the Sentinel-1 retrieved SSWS by different methods.

4 Conclusions

In this paper, the SSWS retrieval methods including conventional and neural network methods were studied and compared based on Sentinel-1 images acquired at HH polarization. The hybrid of four PR models (Mouche-PR1 models, Mouche-PR2 model, Zhang-PR model and Liu-PR model) transforming NRCS from HH into VV polarization and CMOD5.N GMF were used to retrieve SSWS. The results suggest that the four PR models are generally in agreement with matched buoy measurements and ASCAT wind products. Among the four PR models, the Zhang-PR model performs better than results achieved using the other three PR models.

In effect, the relationship between HH and VV polarization may be more complicated and can not be simply explained by relating to incident angle, azimuth angle and wind speed as the four PR models do. Thus, in order to directly retrieve SSWS from the HH polarization SAR data, the CMODH model with no need for NRCS transformation may be a more suitable SSWS retrieval way than the PR models. Our comparison results between CMODH and PR models in the study have confirmed that. The conventional methods including the combination of PR models and CMOD5.N GMF and the CMODH function, are all develop based on SAR data (i.e., ENVISAT ASAR and RADARSAT) instead of Sentinel-1 SAR data which may induce inevitable errors in the retrieved SSWS from Sentinel-1 HH-polarization SAR data. Since a nonlinear relationship exists among the NRCS at HH-polarization data, wind direction, SSWS and incident angle as we can see from the various empirical CMODH functions, we tried the BP neural network model to map the nonlinear relationship and retrieve the SSWS based on the Sentinel-1 HH-polarization SAR data. The statistical parameters of the Bias, the RMSE and the SI for the SSWS retrieval using the BP neural network is improved compared to the five conventional methods. The results suggest that the BP neural network model has a potential application in retrieving SSWS from Sentinel-1 images acquired at HH-polarization.

One point needs to be pointed out is that all the retrievals presented above use external wind directions of ASCAT or ERA5

reanalysis data. Both may have bias on estimation of wind direction; therefore, they can further induce biases on retrievals of SSWS. We conducted a simple experiment on testing sensitivity of wind direction estimation on the retrievals of wind speed. A bias of 5° is added to wind direction estimation of ASCAT (Bentamy et al., 2008) for the comparison dataset (used in Fig. 5), and the retrieved SSWS has a bias of 0.06 m/s and 0.08 m/s with the CMODH model and BP neural network method, respectively, compared with the original retrievals.

We are collecting more *in situ* measurements in the Arctic MIZ to further validate and improve the proposed BP neural network method to retrieve SSWS by Sentinel-1 SAR in HH polarization.

Acknowledgements

We thank the European Space Agency for providing the Sentinel-1 data and the EUMETSAT for providing the ASCAT data. We also thank the NDBC for providing buoy data and ECMWF for providing ERA5 dataset.

References

Bentamy A, Croize-Fillon D, Perigaud C. 2008. Characterization of ASCAT measurements based on buoy and QuikSCAT wind vector observations. Ocean Science, 4(4): 265–274, doi: 10.5194/os-4-265-2008

Elfouhaily T. 1996. Physical modeling of electromagnetic backscatter from the ocean surface; application to retrieval of wind fields and wind stress by remote sensing of the marine atmospheric boundary layer [dissertation]. Paris: University Paris VII

ESA (European Space Agency). 2016. Sentinel-1 product specification. https://sentinel.esa.int/web/sentinel/document-library/content/-/article/sentinel-1-product-specification, [2020-2-17]

Hersbach H. 2010. Comparison of C-band scatterometer CMOD5. N equivalent neutral winds with ECMWF. Journal of Atmospheric and Oceanic Technology, 27(4): 721–736, doi: 10.1175/2009JTECHO698.1

Hersbach H, Stoffelen A, de Haan S. 2007. An improved C - band scatterometer ocean geophysical model function: CMOD5. Journal of Geophysical Research, 112(C3): C03006

Horstmann J, Schiller H, Schulz-Stellenfleth J, et al. 2003. Global wind speed retrieval from SAR. IEEE Transactions on Geoscience and Remote Sensing, 41(10): 2277–2286, doi: 10.1109/TGRS.2003.814658

Komarov A S, Buehner M. 2017. Automated detection of ice and open water from dual-polarization RADARSAT-2 images for data assimilation. IEEE Transactions on Geoscience and Remote Sensing, 55(10): 5755–5769, doi: 10.1109/TGRS.2017.2713987

Liu Guihong, Yang Xiaofeng, Li Xiaofeng, et al. 2013. A systematic comparison of the effect of polarization ratio models on sea surface wind retrieval from C-band synthetic aperture radar. IEEE Journal of Selected Topics in Applied Earth Observations and Remote Sensing, 6(3): 1100–1108, doi: 10.1109/JSTARS.2013.2242848

Monaldo F M, Thompson D R, Pichel W G, et al. 2004. A systematic comparison of QuikSCAT and SAR ocean surface wind speeds. IEEE Transactions on Geoscience and Remote Sensing, 42(2): 283–291, doi: 10.1109/TGRS.2003.817213

Moreira A. 1991. Improved multi-look techniques applied to SAR and Scan SAR imagery. IEEE Transactions on Geoscience and Remote Sensing, 29(4): 529–534, doi: 10.1109/36.135814

Mouche A A, Hauser D, Daloze J F, et al. 2005. Dual-polarization measurements at C-band over the ocean: results from airborne radar observations and comparison with ENVISAT ASAR data. IEEE Transactions on Geoscience and Remote Sensing, 43(4): 753–769, doi: 10.1109/TGRS.2005.843951

Olivier P, Vidal-Madjar D. 1994. Empirical estimation of the ERS-1 SAR radiometric resolution. International Journal of Remote Sensing, 15(5): 1109–1114, doi: 10.1080/01431169408954144

Peixoto J P, Oort A H. 1992. Physics of Climate. New York: American Institute of Physics, 67

Pierson Jr W J. 1990. Examples of, reasons for, and consequences of the poor quality of wind data from ships for the marine boundary layer: Implications for remote sensing. Journal of Geophysical Research, 95(C8): 13313–13340, doi: 10.1029/JC095iC08p13313

Pond S, Pickard G L. 1983. Currents with friction; wind-driven circulation. In: Pond S, Pickard G, eds. Introductory Dynamical Oceanography. 2nd ed. Amsterdam: Elsevier, 100–162

Quilfen Y, Chapron B, Elfouhaily T, et al. 1998. Observation of tropical cyclones by high-resolution scatterometry. Journal of Geophysical Research, 103(C4): 7767–7786, doi: 10.1029/97JC01911

Richaume P, Badran F, Crepon M, et al. 2000. Neural network wind retrieval from ERS-1 scatterometer data. Journal of Geophysical Research, 105(C4): 8737–8751, doi: 10.1029/1999JC900225

Schwerdt M, Schmidt K, Tous Ramon N, et al. 2014. Independent verification of the Sentinel-1A system calibration. In: Proceedings of 2014 Geoscience and Remote Sensing Symposium. Quebec City, QC, Canada: IEEE

Stoffelen A, Anderson D. 1997. Scatterometer data interpretation: estimation and validation of the transfer function CMOD4. Journal of Geophysical Research, 102(C3): 5767–5780, doi: 10.1029/96JC02860

Thiria S, Mejia C, Badran F, et al. 1993. A neural network approach for modeling nonlinear transfer functions: application for wind retrieval from spaceborne scatterometer data. Journal of Geophysical Research, 98(C12): 22827–22841, doi: 10.1029/93JC01815

Wang Lihua, Lu Peng, Ma Jiapei. 2017. Deriving sea surface wind from synthetic aperture radar based on Fourier transform and neural network. In: Proceedings of the 10th International Congress on Image and Signal Processing. Shanghai: IEEE, 1–6

Yang Yonghong. 2009. Introduction to Synthetic Aperture Radar Ocean Remote Sensing (in Chinese). Beijing: China Ocean Press

Zhang Biao, Mouche A, Lu Yiru, et al. 2019. A geophysical model function for wind speed retrieval from C-band HH-polarized synthetic aperture radar. IEEE Geoscience and Remote Sensing Letters, 16(10): 1521–1525, doi: 10.1109/LGRS.2019.2905578

Zhang Biao, Perrie W, He Yijun. 2011. Wind speed retrieval from RADARSAT-2 quad-polarization images using a new polarization ratio model. Journal of Geophysical Research, 116(C8): C08008

Zhang Biao, Perrie W, Hwang P A, et al. 2010. A new polarization ratio model from C-band RADARSAT-2 fine Quad-Pol imagery. In: Proceedings of 2010 IEEE International Geoscience and Remote Sensing Symposium. Honolulu, HI, USA: IEEE, 1948–1951